Chapter 8

# Appendices

Jose Ignacio Huertas

Additional information is available at the end of the chapter

http://dx.doi.org/10.5772/62017

## 1. Appendix A

### 1.1. Heating Effects

The aim of this appendix is to study the heat transfer process occurring during condensation. The motivation for such study comes from the uncertainty in the applicability of the *growth laws* to the case of a supersaturated vapor condensing over very small particles. These growth laws obtained assuming constant temperature. However, when condensation takes place at very high rates, the latent heat released may increase the temperature of the particle by several degrees. Then, considering that

- the rate of condensation is proportional to the net difference in partial pressure of the condensing material in the environment and at the surface of the particle ($P_\infty$-$P_p$);
- the partial pressure at the surface of the particle is equal to the saturation pressure of the vapor ($P_p$= $P_s$), when the Kelvin effect is neglected; and
- the saturation pressure has a very strong dependence with temperature ($P_s = a*T^n$, where a and n are constants, n~11 for NaCl),

it can be concluded that any small change in particle temperature could affect the rate of particle growth substantially. Dealing with condensation in the CR, it is common to argue that the increase in temperature is negligible and then the respective growth laws can be used directly. However, the situation could be very different in the FMR.

A heat transfer model has been developed to evaluate the extent of particle heating during the process of condensation in both the CR and FMR.

The system is a uniform liquid phase spherical droplet embedded in a supersaturated vapor. The initial conditions are same temperature for particle and vapor, and particle size slightly greater than the critical size for condensation.

Since the vapor concentration profile near the particle approaches a steady-state condition before appreciable growth occurs, the steady-state diffusional flux may be used to calculate the particle growth rate. As growth proceeds hundreds of times slower than diffusion, the profile near the particle remains close to its steady-state value at all times, whereas the transient region propagates farther from the particle.

| S | $\tau_D$[s] | $\tau_{cond}$[s] | $\tau_{HT}$[s] | Biot | r*[nm] |
|---|---|---|---|---|---|
| 1.010 | 2.05x10-10 | 2.71x10-3 | 2.71x10-3 | 2.47x10-2 | 70.1 |
| 1.125 | 1.47x10-12 | 1.74x10-5 | 1.73x10-10 | | 5.92 |
| 1.500 | 1.24x10-13 | 1.10x10-6 | 1.46x10-11 | | 1.72 |

$\tau_{HT} = r^2/\alpha_p$ Characteristic heat transfer time inside of the particle

$\tau_D = r^2/D$ Characteristic diffusion time of NaCl vapor in Ar

**Table 1.** Characteristic times for a Ti/NaCl/Ar aerosol at 1100°C.

An energy balance describes the effects of latent heat release by condensation at the particle surface. Heat conduction occurs toward both the particle interior and the exterior gas phase. The ratio of the characteristic times for conduction within the droplet and the characteristic time for heat transfer in the gas phase is known as the *Biot number*, which can also can be interpreted as the ratio of the respective thermal resistances. The Biot number provides a measure of the temperature drop in the droplet relative to the temperature difference between the droplet surface and the gas phase:

$$Bi = \frac{2hr}{k_p} \tag{1}$$

where $h$ is the convective heat transfer coefficient, and $k_p$ is the thermal conductivity of the particle. Table l shows values for the characteristic time for conduction within the droplet and the Biot number for several conditions of supersaturation. Table l shows that the Biot number is of the order of O.O1 for the NaCl droplet in Ar at high temperatures (T~1100°C).

For Bi << 1 the resistance to conduction within the solid is much less than the resistance to convection across the fluid boundary layer. Hence, it can be assumed that the temperature within the so1id is uniform at any given time.

**Heat Transfer in the CR**

With this assumption, the energy conservation equation for the liquid droplet system can be expressed as:

$$\frac{\rho H_v}{M}\frac{dv}{dt} = \frac{\rho v C_p}{M}\frac{dT}{dt} + hA\left(T - T_\infty\right) \tag{2}$$

http://dx.doi.org/10.5772/62017

where ϱ is the particle density, $H_v$ is the latent heat of condensation, υ is the volume of the particle, $C_p$ is the heat capacity of the particle, M is the molecular weight of NaCl, *h* is the convective heat transfer coefficient, and A is the particle surface area.

The term on the left of Equation (2) represents the latent heat released during condensation; The first term on the right represents the energy absorbed by the particle in increasing its temperature, and the second term represents the energy dissipated by convection.

For convective heat transfer of a single sphere with a stagnant environment, the Nusselt number is equal to 2, ($N_u$ = 2). Hence, the convective heat transfer coefficient *h* is equal to the thermal conductivity of the gas ($K_g$), divided by the radii of the sphere $h=K_g/r$.

Nondimensionalizing partic1e size as $\eta=r/r^*$, where r* is critical size for condensation; temperature as $\Psi= (T-T\infty) / \zeta$ where $\zeta=3H_v/C_p$; and time as $\tau=t/\tau_{cond}$, the energy equation reduces to:

$$\frac{d\Psi}{d\tau} = \frac{1}{\eta}\frac{d\eta}{d\tau} - \xi_{CR}\frac{\Psi}{\eta^2} \tag{3}$$

where the parameter $\xi_{CR}$ is given by:

$$\xi_{CR} = \frac{3MK_g\tau_{cond}}{\rho C_p r^{*2}} \tag{4}$$

The rate of growth equation for condensation in the CR in its nondimensional form is reprinted here for the reader's convenience:

$$\frac{d\eta}{d\tau} = \frac{1}{Ln(S)}\frac{1}{\eta}\left(1 - S^{\frac{1}{\eta}-1}\right) \tag{5}$$

The energy equation and the growth rate equation need to be solved numerically, subject to the initial conditions Ψ = 0 and η = 1.00001.

The first and simplest approach to evaluate the increase in particle temperature during condensation is to assume that the vapor concentration at the surface of the particle is un influenced by the change in the particle temperature. Results obtained through this assumption are the upper limit of the real situation. Then, if the increase in temperature is minimum $\delta T<<1$, the model would prove that the assumption of constant temperature is a good assumption. If that is not the case, the temperature dependence of vapor phase concentration at the surface of the particle needs to be included.

Equations (3) and (5) were solved numerically for different values of the parameter $\xi_{CR,}$ assuming that the rate of condensation is uninfluenced by the increase in particle temperature. The actual increase in particle temperature is determined by the parameter $\xi_{CR}$ and $\zeta$. $1/\zeta$ is the fraction of the energy released that is used to increase the particle temperature, while $\xi_{CR}$ is the ratio of the energy dissipated by conduction and the energy required to increase particle temperature. Higher values of $\xi_{CR}$ means that more energy can be dissipated per degree of particle temperature increased, and therefore lower $\delta$Ts for the same rate of energy release.

For NaCl at 1100°C, $\zeta$=7650.1. Table 2 shows typical values for $\xi_{CR.}$ For these values, Figure 1 shows the increase in particle temperature during NaCl condensation in the CR. Figure 1 shows that particle heating is a function of particle size. These can be explained as follows: At any given time, a gradient of temperature $\delta T = T_p - T_\infty$ is established such that the rate of energy dissipation by convection, which is proportional to $\delta$T, balances the rate of heat release. The rate of heat release is proportional to the rate of condensation. In the CR, the rate of condensation is a function of particle size. Consequently, temperature increase in the CR is a function of particle size.

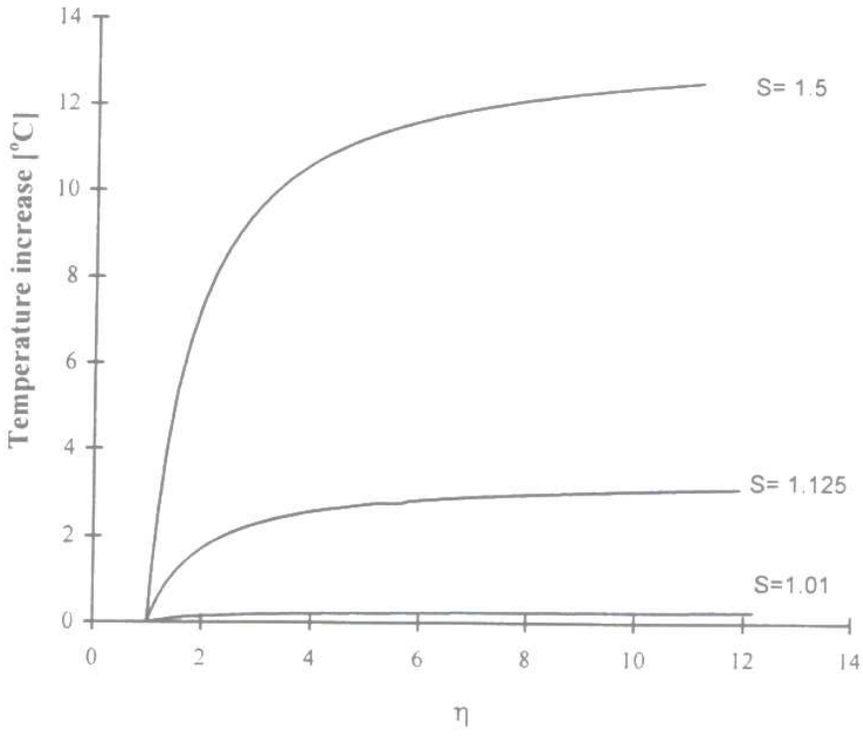


**Figure 1.** Increase in particle temperature during NaCl condensation in the CR for different values of S assuming that the rate of condensation is uninfluenced by the increase in particle temperature.

Table 2 shows the increase in temperature when the particle has grown 10 times its initial size by condensation. $\delta$T is small for S<1.5 and therefore it can be concluded that the assumption of constant temperature during condensation of NaCl in the CR is acceptable for low rates of condensation.

http://dx.doi.org/10.5772/62017

| S | $\xi_{CR}$ | $\Psi_{10}$ | δT |
|---|---|---|---|
| 1.010 | $2.82x10^{4}$ | $3.18x10^{-5}$ | 0.24 |
| 1.125 | $2.14x10^{3}$ | $3.99x10^{-4}$ | 3.05 |
| 1.500 | $4.65x10^{2}$ | $1.62x10^{-3}$ | 12.4 |

**Table 2.** Temperature increase during condensation in the CR. For NaCl particles starting with size r* and ending with 10 times their initial size, assuming that the rate of condensation is unaffected by the increase in particle temperature.

## Heat Transfer in the FMR

Particle heating during condensation in the FMR is enhanced because thermal conduction in the FMR is not as good as in the CR. Conduction of heat in the FMR follows very different laws from those obeyed under ordinary circumstances. References 84, 85, 86, and 87 are frequently used references in this respect.

Expressions for thermal conduction from a single sphere toward its environment in stagnant conditions are obtained from the kinetic theory of gases. On it, the area surrounding the particle is divided in two zones. The inner zone is of the width of one mean free path, and transport occurs at collisionless rates. This is known as the Langmuir zone. At larger distances, transport processes involve many collisions and follow the CR description. The heat flux due to conduction across the Langmuir layer is given by [84]:

$$\frac{q}{A\delta T} = \frac{1}{2}(\gamma+1)\frac{C_v P}{\sqrt{\frac{2\pi RT}{M}}} = \frac{K_k}{r} \tag{6}$$

where A is surface area, q is heat flux, $\gamma = C_p/C_v$ is the ratio of specific heat capacities, and $K_k$ is an equivalent thermal conductivity as given by the kinetic theory. Equation (6) states that in the FMR, conduction is proportional to the pressure of the gas, and dependent only upon shape but not size of the bounding surfaces.

Replacing the conduction term of Equation (1) by the expression for conduction in the FMR (Equation (6)), the energy balance for condensation in the FMR is:

$$\frac{d\Psi}{d\tau} = \frac{1}{\eta}\frac{d\eta}{d\tau} - \xi\frac{\Psi}{\eta} \tag{7}$$

$$\xi = \frac{3MK_k\tau_{cond}}{\rho C_p r^*} \tag{8}$$

and the condensation rate in the FMR is:

$$\frac{d\eta}{d\tau} = \frac{1}{Ln(S)}\left(1 - S^{\frac{1}{\eta}-1}\right) \tag{9}$$

where the same type of nondimensionalization has been used as for the CR case. Figure 2 shows the numerical solution of Equations (7) and (9) subject to the initial conditions $\Psi = O$ and $\eta = 1.00001$. Again it has been assumed that particle heating does not affect the rate of condensation.

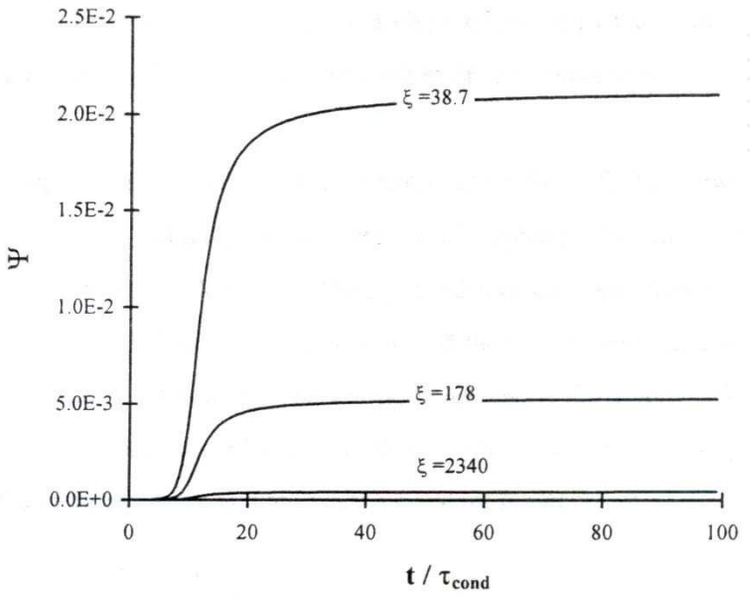


**Figure 2.** Increase in particle temperature during condensation in the FMR for different values of ξ assuming that the rate of condensation is uninfluenced by the increase in particle temperature.

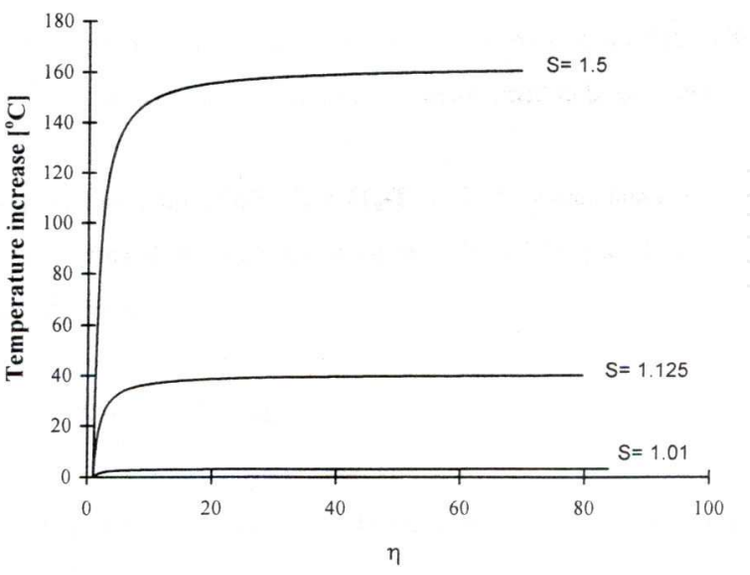


**Figure 3.** Actual particle temperature increase during condensation of NaCl at 1100°C in the FMR. For different saturation ratios, assuming that the rate is uninfluenced by the increase in particle temperature.

http://dx.doi.org/10.5772/62017

Figure 2 shows that the nondimensional temperature reaches a steady-state value $\Psi_\infty$. This steady-state condition is reached when the Kelvin effect ceases and the rate of condensation becomes constant. This behavior can be explained in the following way.

At any time during condensation, a gradient of temperature $\delta T = T_p - T_\infty$ is established such that the rate of energy dissipation, which is proportional to $\delta T$, balances the rate of heat release, which is proportional to the rate of condensation. During condensation controlled by the Kelvin effect, the rate of condensation is a function of particle size and then the temperature of the particle is also a function of particle size. However, when the particles grow, the Kelvin effect becomes negligible and the rate of condensation independent of particle size. Consequently, despite further condensation, the particles reach and maintain a constant temperature.

Equation (3) shows the actual increase in particle temperature for several conditions of super saturation of NaCl at 1100°C. It shows that even for low values of S, the increase of particle temperature is substantial. Therefore, a heat transfer analysis that includes the effect of particle heating on the rate of condensation is required.

Saturation pressure can be expressed as $P_s = a*T^n$, where a and n are constants. Then the saturation ratio can be expressed as $S=S_\infty(T/T_\infty)^n$,where the subscript ∞ refers to the properties of the aerosol far away from the particle. Properties at ∞ are assumed to be constant.

$(T/T_\infty)^n$ can be expressed in terms of $\delta T/T_\infty=(T_p-T_\infty)/T_\infty$ by expanding it in Taylor series and neglecting higher-order terms. The resulting expression is $S=S\infty*Exp(-n\,\delta T/T\infty)$. In terms of the nondimensional variable Ψ and ζ:

$$S = S_\infty * Exp(-n\zeta\Psi) \tag{10}$$

Incorporating this expression into the energy and condensation equation, nondimensionalizing in the same fashion as before but with respect to the properties at ∞, the energy and condensation equations become:

$$\frac{d\Psi}{d\tau} = \frac{1}{\eta}\frac{d\eta}{d\tau} - \xi\frac{\Psi}{\eta} \tag{11}$$

$$\frac{d\eta}{d\tau} = \frac{1}{Ln(S_\infty)} Exp\left(-\frac{\gamma\Psi}{2T_\infty}\right)\left[1-\left(S_\infty * Exp\left(\frac{-n\gamma\Psi}{T_\infty}\right)\right)^{\frac{1}{\eta}-1}\right] \tag{12}$$

Now the condensation equation is coupled to the energy equation and vice versa. Figure 4 shows the results after integrating simultaneously the two equations subject to the initial conditions Ψ = O and η = 1.00001, for $\zeta/T_\infty = 5.57$ and the values of ξ corresponding to S = 1.01, 1.125, and 1.5.

The behavior of the particle temperature is similar to that already described, except that the steady-state temperature is ~4 times less. Table 3 compares the values obtained with and

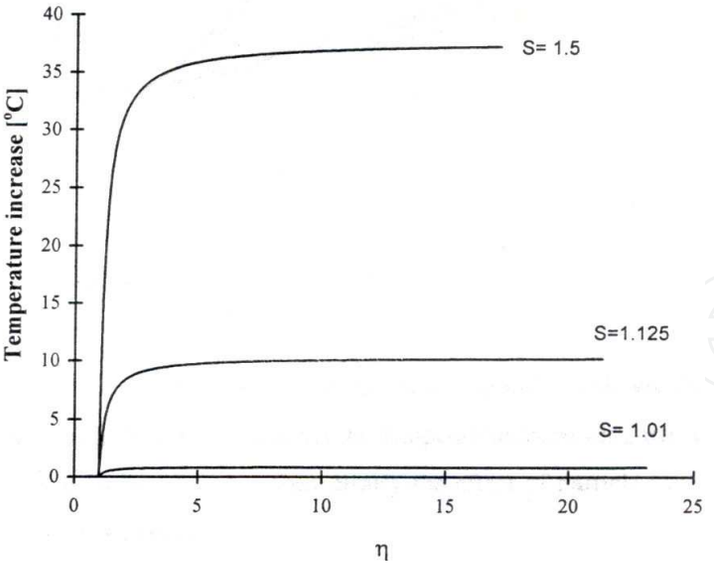


**Figure 4.** NaCl condensation in the FMR for different values of S including the effect of particle heating in the rate of condensation.

without correction for temperature. It shows that particle heating due to condensation is substantial for higher values of $S_\infty$.

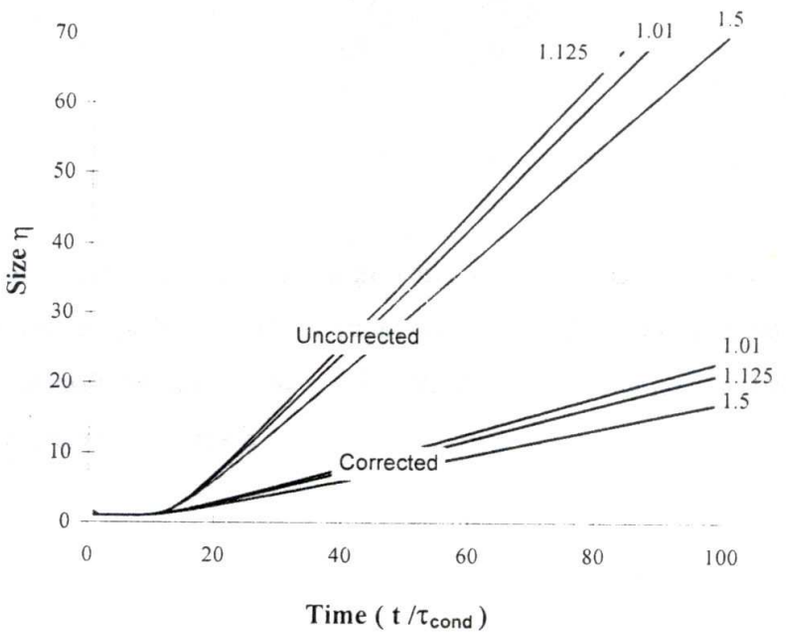


**Figure 5.** Effect of particle heating on particle growth.

Figure 5 shows the effect of particle heating on particle growth. It shows that particle growth has the same profile with and without correction for temperature; however, particle heating decreases the rate of growth by a factor of ~4. Then, clearly the effect of particle heating on the rate of condensation in the FMR is important.

http://dx.doi.org/10.5772/62017

| $S_\infty$ | $\xi$ | $\tau_{cond}$ | m | $\delta T$ | $m_{w/o}/m$ | $\delta T_{w/o}/\delta T$ |
|---|---|---|---|---|---|---|
| 1.01 | 2340 | $2.71 \times 10^{-3}$ | 0.25 | 0.81 | 3.92 | 3.8 |
| 1.125 | 178 | $1.74 \times 10^{-5}$ | 0.23 | 9.86 | 4.03 | 3.9 |
| 1.5 | 38.7 | $1.10 \times 10^{-6}$ | 0.18 | 37.5 | 4.49 | 4.3 |

m = rate of condensation in the FMR when the Kelvin effect becomes ineffective

w/o = without correction for particle heating

**Table 3.** Values for condensation in the FMR with correction for particle heating.

Figure 5 can be used to evaluate particle growth in the FMR for any starting size and a given $\delta t$ by using:

$$\delta\eta = \int_{t_o}^{t_o+\delta t} \frac{d\eta}{dt} dt = \int_{0}^{t_o+\delta t} \frac{d\eta}{dt} dt - \int_{0}^{t_o} \frac{d\eta}{dt} dt \tag{13}$$

$$\delta\eta = \eta_{0-\tau_o+\delta t} - \eta_{0-\tau_o} \tag{14}$$

where $\eta_{o\text{-}\tau}$ is the tabulated universal value for growth due to condensation during $\tau$ nondimensional times. Equation (13) is in general not valid because condensation is coupled to the energy equation. Particle growth depends on the particle temperature and in general particles of the same size could have different temperatures.

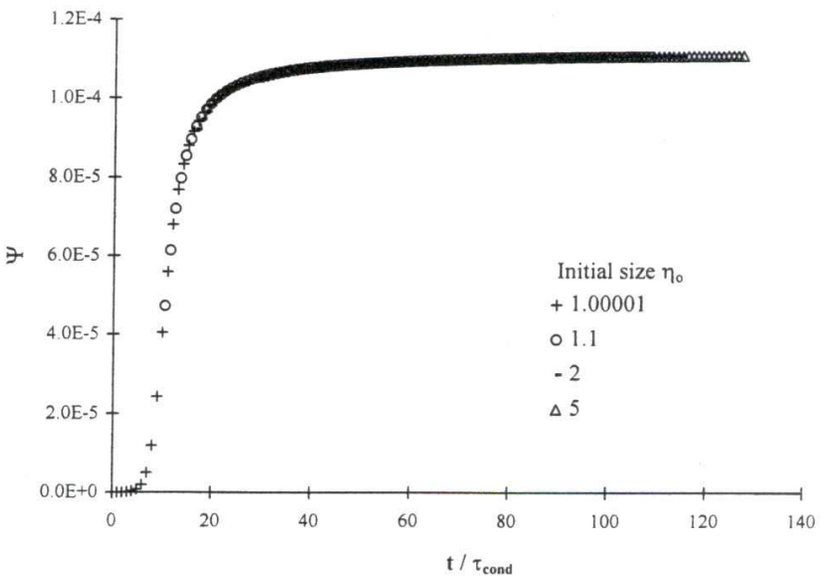


**Figure 6.** Particle temperature and size for the same conditions but different initial size. Particles of the same size have the same temperature.

However, for situations where ζ<<1 and Bi<<l, as in the case of NaCl condensation over nanosize particles, Equation 13 is still valid because a) the amount of energy required to heat up the particle is negligible compared to the energy available (ζ<<l) and b) the rate of particle heating is instantaneous (Bi<<l). Therefore, particles of the same size have the same temperature regardless of how much condensation was received, as long as there has been some condensation. Figure 6 shows this behavior. For the same conditions but different initial size, particle temperature is only a function of particle size.

## 2. Appendix B

### 2.1. Sintering

The theory of sintering of solid particles or highly viscous fluids is based in the interaction of two equal-sized spheres. At the contact point of the two spheres, a neck is formed whose size grows with time. For the initial stage, the rate of growth is driven by the curvature gradients in the neck region. At intermediate sintering rates, the curvature gradient diminishes and the surface free energy becomes the driving force for continued sintering. At this stage, the motion is induced by the tendency of the interface to reduce its area in order to minimize the interfacial energy. [88]

For the initial stage of the sintering process, the kinetic model formulated by Frenkel 89 and generalized by German and Muir [88] has shown good agreement with experimental values obtained during sintering studies of various materials. On it, the rate of surface area reduction is given by:

$$\frac{da}{dt} \sim -\frac{1}{\tau_f}(a - a_f)^{\gamma-1} \tag{15}$$

where $a$ is the surface area of the aggregate, $a_f$ the surface area of the completely fused single sphere of the same volume, $\gamma$ is a constant, and $\tau_f$ is the characteristic fusion time. The values of $\gamma$ and $\tau_f$ depend on the underlying sintering mechanism. Table 1 shows some of the possible sintering mechanism and values of $\gamma$ for each of them.

Hiram and Nir [90] developed a numerical solution for the equations of motion describing the coalescence of two particles by the viscous flow mechanism. The results show similar behavior for all particle size to fluid viscosity ratios. The sintering behavior displays three regions of evolution: an initial transitory stage followed by an intermediate pseudo-Frenkel stage. Beyond these two short states, particles assume their spherical shape following a first-order exponential decay.

http://dx.doi.org/10.5772/62017

$$\frac{da}{dt} \sim -\frac{1}{\tau_f}(a - a_f) \tag{16}$$

In this case, the characteristic time for coalescence $\tau_f$ is the time required to reduce 63% the excess agglomerate surface area over that of a spherical particle with the same mass.

Koch and Friedlander [91] assumed that the linear growth rate, Equation (1), holds for the solid-state diffusion mechanism, and obtained an expression for $\tau_f$. Table 1 shows the type of expressions obtained and some of the expressions used by several authors in the study of gas phase particle synthesis when coalescence is the rate-controlling process. On this type of work, the authors assume that the very small particles grow by single particle collision and almost instantaneously coalesce until they become large enough to exhibit macroscopic viscosity and surface tension.

For the rate of sintering of Ti at $T<T_m$, it is assumed that the rate of sintering is due to solid-state diffusion. Since information about self-diffusion as a function of temperature is not available for Ti, the respective information for C in HCP Ti has been used [92] as a first approximation. The values obtained are reported in Table 2. The results show that the rate of sintering of Ti is high up to particles of size r~1O nm, but it is a strong function of temperature. The rate of sintering by viscous flow is reported in Table 2 for NaCl. It shows that liquid NaCl particles sinter extremely fast.

| Mechanism | Equation (1) | | Equation (2) | | |
|---|---|---|---|---|---|
| | γ | δγ | $\tau_f$ | Material | Expression Used |
| Viscous | 1.1 | ± 0.1 | $\frac{2\mu r_f}{\sigma}$ [89] | $SiO_2$ [93] | $6.5x10^{15}$ d Exp($8.3x10^4$/T) |
| Evaporation/Condensation | 1.6 | ± 0.1 | $\frac{3KTv}{64\pi D\sigma v_m}$ [94] | | |
| Solid-state diffusion | | | | | |
| Volume diffusion | 2.7 | ± 0.1 | | $B_4C$ [95] | 39 T $d^3$ Exp(53 648/T) |
| Grain boundary diffusion | 3.3 | ± 0.1 | | $TiO_2$ [93] | $7.4x10^8$ T $d^4$ Exp($3.1x10^4$/T) |
| Surface diffusion | 3.6 | ± 0.1 | | | |

T absolute temperature

$v$ particle volume

D solid-state diffusion coefficient

d particle diameter of the sintered particle

σ surface tension

$v_m$ molecular volume

**Table 4.** Sintering mechanisms and different expressions for the characteristic time.

| Size r [nm] | $\tau_{sint}$ [μs] | | | |
|---|---|---|---|---|
| | 1100°C | | 800 °C | |
| | Ti (c) | NaCl (l) | Ti (c) | NaCl (l) |
| 3.8 | $1.21x10^{-2}$ | $3.73x10^{-4}$ | $4.14x10^{-1}$ | $3.18x10^{-3}$ |
| 5.9 | $4.48x10^{-2}$ | $5.78x10^{-3}$ | $1.55x10^{0}$ | $4.94x10^{-3}$ |
| 15.0 | $7.11x10^{-1}$ | $1.45x10^{-2}$ | $2.55x10^{1}$ | $1.26x10^{-2}$ |
| 50.0 | $2.70x10^{1}$ | $4.88x10^{-2}$ | $9.44x10^{2}$ | $4.19x10^{-2}$ |
| 100.0 | $2.16x10^{2}$ | $9.77x10^{-2}$ | $7.55x10^{3}$ | $8.37x10^{-2}$ |

**Table 5.** Characteristic time for sintering of Ti particles in crystal phase and NaCl in liquid phase at 1100°C.

# 3. Appendix C

## 3.1. Particle Dynamics in a Colloidal System

A colloid is an entity dispersed in a medium, having at least one dimension between 1 nm and 1 μm. The entity may be solid or liquid or, in some cases, even gaseous. A solid colloid dispersed in a liquid medium is known as sol or dispersion. However, the term "colloid" is generally used for the system as a whole.[96, 97]

Particles in a liquid medium possess Brownian motion and therefore eventually collide. The theory of coagulation due to Brownian motion may be applied to the colloidal system to determine how fast the particles collide. The resistance of the liquid phase to the motion of a spherical particle is proportional to the size of the particle and the hydrodynamic nature of the liquid phase. That relation is well known as the Stokes formula:

$$F_{M=-6\pi\mu rV} \tag{17}$$

where μ is the viscosity of the fluid, r is the particle size, and V is the particle velocity. The ratio of the velocity of the particle V to the force causing its motion $F_M$ is called mobility (B) of the particle. B is the drift velocity that is attained under unit external force. In some other areas the quantity $f=1/B=6\pi\mu r$. It is more popular and it is known as the Stokes friction coefficient. On the other hand, the diffusivity (D) of a particle of size $r_i$ in the liquid medium is given by:

$$D_i = \frac{KT}{f_i} \tag{18}$$

and the collision frequency function β is given by:

http://dx.doi.org/10.5772/62017

$$\beta = 4\pi(D_i + D_j)(r_i + r_j) \tag{19}$$

Finally, the collision frequency of the solid particles in the colloidal system is given by:

$$Z_{ij} = \beta_{ij} n_i n_j \tag{20}$$

where N◎ is the concentration of particles of size r◎. Replacing Equations 1, 2, and 3 in Equation 4, an explicit expression for the frequency of collision can be obtained. Considering a colloidal system, made of two equal-sized particles (r) embedded in a liquid droplet of size R, the characteristic collision time $\tau B$ =N/Z reduces to:

$$\tau_B = \frac{\mu\pi R^3}{8KT} \tag{21}$$

The characteristic collision time $\tau_B$ for the colloidal system estimates the average time required for two particles to collide. This definition neglects the enhancing effect in the collision frequency of having the two particles housed within the boundaries of the liquid material. However, it gives a good first estimate. $\tau_B$ is independent of particle size, and is linearly proportional to the volume available for particle motion. For NaCl at 800°C and ll00°C, Table 1 shows typical values for $\tau_B$.

| NaCl droplet Size R [nm] | $\tau_B$ [μs] | |
|---|---|---|
| | 1100°C | 800°C |
| 10 | $9.38x10^{-1}$ | $1.27x10^{0}$ |
| 25 | $1.47x10^{1}$ | $1.98x10^{1}$ |
| 50 | $1.17x10^{2}$ | $1.58x10^{2}$ |
| 100 | $9.38x10^{2}$ | $1.27x10^{3}$ |

**Table 6.** Characteristic time for collision of 2 Ti cores embedded within a NaCl liquid droplet of size R.

## Author details

Jose Ignacio Huertas

Address all correspondence to: jhuertas@itesm.mx

Tecnológico de Monterrey, Mexico

## References


[1] Suryanarayana, C., and Froes, F.H. *Metallu Trans A.* 23A:1071-1081. (1992).

[2] Birringuer, R. Nanocrystalline Materials. *Mater Sci Engin A.* 117:33-43. (1989).

[3] Gleiter, H. Materials with Ultrafine Microstructures: Retrospectives and Perspectives. *Nano Struct Mater.* 1:1-19. (1992).

[4] Cohen, M. Progress and Prospects in Metallurgical Research. *Advancing Material Research.* Washington D.C. Pp. 51-110. (1987).

[5] Gleiter, H. *Progr Mater Sci.* 33:223-315. (1989).

[6] Nieman, G.W., Weertman, J.R., and Siegel, R.W. *Scri. Metal.* 24:145. (1990).

[7] Suryanarayana, C., and Froes, F.H. Nanocrystalline Metals: A Review. *Physical Chemistry of Powder Metals. Production and Processing.* Pp. 279-296. (1989).

[8] Courtney, T.H. *Mechanical Behavior of Materials.* McGraw-Hill. New York. (1990).

[9] Birringer, R., Bohn, R.W., and Weertman, J.R., *Mater Sci Engin A.* 153:679. (1993).

[10] Nieman, G.W., Siegel, R.W., and Weertman, J.R. *J Mater Res.* 6:1012. (1991).

[11] Siegel, R.W., and Hahn, H. Current Trends in Physic of Materials. In *World Scientific.* Singapore. Pp. 403. (1987).

[12] Ashley, S. Small-Scale Structure Yields Big Property Payoffs. *Mechanical Engineering.* February. Pp. 52-57. (1994).

[13] Stiglich, J.J., Sudarshan, T.S., and Dowding, R.J. *Synthesis and Consolidation of Nanoparticles.* U.S. Army Research Laboratory. AD-A238 314. (1994).

[14] Simon, C. Stabilization of Aqueous Powder Suspensions in the Processing of Ceramic Materials and Advanced Materials, in *Coagulation and Flocculation, Theory and Applications.* Ed. Dobias, B., Marcel. D. Inc. New York. Pp. 487. (1993).

[15] Niihara, K. *Cera Soc Jpn.* 99:974. (1991).

[16] Zachariah, M.R. Principles of Gas Phase Processing of Ceramics During Combustion. Pp. 71-76. (1994).

[17] Kingery, W.D., Bowen, H.K., and Uhlmann, D.R. *Introduction to Ceramics.* Wiley. New York. (1976).

[18] Matteazzi, P. Basset, D., Miani, F., and Le-Caer, G. Mechanosynthesis of Nanophase Materials. *Nanostr Mater.* 2:217-229. (1993).

[19] Gurav, A., Kodas, T., Pluym, T., and Xiong Y. Aerosol Processing of Materials. *Aerosol Sci Technol.* 19:411-452. (1993).

[20] Uyeda, R. Studies of Ultrafine Particles in Japan: Crystallography, Methods of Preparation and Technological Applications. *Progr Mater Sci.* 35:1-96. (1991).

[21] Chorley, R.W., and Lednor, P.W. Synthetic Routes to High Surface Area Non-Oxide Materials. *Adv Mater.* 3:10:474-485. (1991).

[22] Lamprey, H., and Ripley, R.L., *J Electrochem Soc.* 109:8:713-715. (1962).

[23] Pratsinis, S.E., and Kodas, T.T., Manufacturing of Materials by Aerosol Processes. In *Aerosol Measurement: Principles, Techniques, and Applications.* Pp. 721-746. (1993).

[24] Flagan, R.C., and Wu, J.J. Aerosol Reactor Production of Uniform Submicron Powders. *Patent No. 248486.* (1991).

[25] Zachariah, M.R., and Dimitriou, P. *Aerosol Sc Technol.* 13:413-425. (1990).

[26] Axelbaum, R.L., DuFaux, O.P., and Rosen, L.J. *Patent No. 5498446.* (1995).

[27] Magness, L.S., and Farrand T.G. *Army Science Conference.* (1990).

[28] Ryan, K.F., and Dowding, R.J. *Army Research Laboratories.*ARL-TR-143. (1993).

[29] Schubert, W.D. *Refractory Metals and Hard Materials.* 11:151-157. (1992).

[30] Williams, B.E., Stiglich, J.J., and Kaplan R.B. Coated Tungsten Powders For Advance Ordinance Applications. *US Army Materials Technology Laboratory.* MTL TR. Pp. 92. (1992).

[31] German, R.M., Tungsten and Tungsten Alloys. *Proceedings of the First International Conference on Tungsten and Tungsten Alloys.* Metal Powder Industry Federation. New Jersey. Pp. 3. (1993).

[32] Raghunathan, S., Bourell, D.L., and Persad, C. Microcomposites and Nanophase Materials. *The Minerals, Metals* & *Materials Society.* Pp. 81. (1991).

[33] Kecskes, L.J., and Hall, I.W. *Proceedings of the First International Conference on Tungsten and Tungsten Alloys.* Metal Powder Industry Federation. New Jersey. Pp. 155. (1993).

[34] Hessel, S., Shpigler, B., and Botstein, O. *Rev Chem Engin.* 9:3-4:345-364. (1993).

[35] Kear, B.H., and McCandlish, L.E. *J Adv Mater.* October. Pp.11-19. (1993).

[36] Currie, A.L., and Howard, K.E. *J Mater Sci.* 27:2739-2742. (1992).

[37] Belkacem, A., Arnal, Y., and Pelletier, J. *Thin Solid Films.* 241:301-304. (1994).

[38] Evans, R. D., and Leet, D.M. *J Electrochem Soc.* 141: 7:1867-1871. (1994).

[39] Hojo, J., Oku, T., and Kato, A. *J Less Common Metals.* 59:85-95 (1978).

[40] Smiley, S.H., Brater, D.C., and Kaufman, H.L. *J Metals.* June. Pp. 605. (1965).

[41] Revankar, V., Zhao, G.Y., and Hlavacek, V. *Ind Eng. Chem. Res.* 30:2344. (1991).

[42] DuFaux, O.P., and Axelbaum, R.L. *Combust Flame.* 100:350-358. (1995).

[43] Axelbaun, R.L., Lottes, C.R., Huertas, J.I., and Rosen L. To be published in *Twenty-Fifth Symposium International on Combustion.* (1996).

[44] Gould, R.K., and Dickson, C.R. *Patent No. 5021221.* (1991).

[45] Calcote, H.F., and Felder, W. *Twenty-Fourth Symposium International on Combustion.* Pp.1869-1876 (1994).

[46] Glassman, I, Davis, K.A., and Brezinsky, K. *Twenty-Fourth International Symposium on Combustion.* Pp. 1-14. (1994).

[47] Steffens, K.L., Zacbariah, M.R., DuFaux, D.P., and Axelbawn, R.L. To be published. (1996).

[48] Massalski, T.B. *Binary Alloys Phase Diagrams.*2nd Ed. New York. (1990).

[49] Cullity, B.O. *Elements of X-ray diffraction.* 2nd Ed. MA. (1977).

[50] Friedlander, S.K. *Smoke, Dust and Haze.* John Wiley & Sons. New York. (1977).

[51] Suck, S.H, and Brock, J.R. *J Aerosol Sci.* 10:581-590. (1979).

[52] Friedlander, S.K., and Wang, C.S. The Self-Preserving Particle Size Distribution for Coagulation by Brownian Motion. *J Colloid Interf Sci.* 22:126-132. (1966).

[53] Lee, K.W., Chen, H., and Gieseke, J.A. *Aerosol Sci Technol.* 3:53 (1984).

[54] Gelbard, F., Tambour, Y., and Seinfeld, J.H. Sectional Representations for Simulating Aerosol Dynamics. *J Colloid Interf Sci.* 76:2:541-556. (1979).

[55] Husar, R.B. *Coagulation of Knudsen Aerosols.* Ph.D. dissertation. University of Minnesota. (1971).

[56] Kaplan, C.R., and Gentry, J.W. Agglomeration of Chain-Like Combustion Aerosols Due to Brownian Motion. *Aerosol Sci Technol.* 8:11-28. (1988).

[57] Gelbard, F., and Seinfeld, J.H. *J Colloid Interf Sci.* 68:363. (1979).

[58] Gelbard, F., and Seinfeld, J.H. Simulation of Multicomponent Aerosol Dynamics. *J Colloid Interf Sci.* 78:2:485-501. (1980).

[59] Tsang, T.H. and Rao, A. Comparison of Different Numerical Schemes for Condensational Growth of Aerosols. *Aerosol Sci Technol.* 9:271-277. (1988).

[60] Warren, D.R. and Seinfeld, J.H. Simulation of Aerosol Size Distribution Evolution in Systems with Simultaneous Nucleation, Condensation, and Coagulation. *Aerosol Sci Technol.* 4:31-43. (1985).

[61] Gelbard, F. Modeling Multicomponent Aerosol Particle Growth by Vapor Condensation. *Aerosol Sci Technol.* 12:399-412. (1990).

http://dx.doi.org/10.5772/62017

[62] Jacobson, M.Z., and Turco, R.P. Simulating Condensational Growth, Evaporation.and Coagulation of Aerosols Using a Combined Moving and Stationary Size Grid. *Aerosol Sci Technol.* 22:73-92. (1995).

[63] Gelbard, F., and Seinfeld, J. Exact Solution of the General Dynamic Equation for Aerosol Growth by Condensation. *J Colloid Interf Sci.* 28:1:173-183. (1978).

[64] Seinfeld, J.H. *Atmospheric Chemistry and Physics of Air Pollution.* John Wiley & Sons. New York. (1986).

[65] Siegel, R., and Howell, J.R. *Thermal Radiation Heat Transfer.* 2nd Ed. Washington. (1981).

[66] Shreider, Y.A. *The Monte Carlo Method* Pergamon Press. New York. (1966).

[67] Schaad, L.J. The Monte Carlo Integration of Rate Equations. *J Am Cera Soc.* 85:3588-3592. (1963).

[68] Kaplan, C.R., and Gentry, J.W. Agglomeration of Chain-Like Combustion Aerosols due to Brownian Motion. *Aerosol Sci Technol.* 8:11-28. (1988).

[69] Akhtar, M.K, Lippscomb, G.G., and Pratsinis, S.E. Monte Carlo Simulation of Particle Coagulation and Sintering. *Aerosol Sci Technol.* 21:83-93 (1994).

[70] Sutherland, D.N. A Theoretical Model of Floc Structures. *J Colloid Interf Sci.* 25; 373-380. (1967).

[71] Kemeny, J.G, and Snell, J.L *Finite Markov Chains.* New York. (1960).

[72] Levine, J., Levine, M., Negus, C., and Schumer, L. *The UNIX Dictionary of Commands, Terms and Acronyms.* McGraw-Hill. NewYork. (1996).

[73] Hidy, G. M. On the Theory of the Coagulation of Noninteracting Particles in Brownian Motion. *J Colloid Sci.* 20:123-144. (1964).

[74] Lee, K.W., Curtís, L.A. and Chen, H. An Analytic Solution to the Free Molecule Aerosol Coagulation. *Aerosol Sci Technol.* 12:457-462. (1990).

[75] Matsoukas, T. and Friedlander, S.K. Dynamics of Aerosol Agglomerate Formation. *J Colloid Interf Sci.* 146:2. (1991).

[76] Megaridis, C. Morphological Description of Flame generated Materials. *Combust Sci Technol.*71:95-109. (1990).

[77] Akhtar, M.K., Xiong, Y., and Pratsinis, S.E. Vapor Synthesis of Titania Powder by Titanium Tretachloride Oxidation. *AlChE J.* 37:10:1561-1570. (1991).

[78] Law, A.M., and Kelton, W.D. *Simulation Modeling and Analysis.* 2nd Ed. McGraw-Hill. New York. (1991).

[79] Abraham, F.F. *Homogeneous Nucleation Theory.* Academic Press. New York. (1974).

[80] MacDonald. *Am J Phys.* 30:12:870-877. (1962).

[81] MacDonald. *Am J Phys.* 31:1:31-41. (1963).

[82] German, R.M. and Munir, Z.A. Surface Area Reduction During Isothermal Sintering, *JAm Cera Soc.* 59:9-10. (1976).

[83] Dukhin, S.S., Kretzschmar, G., and Mil1er, R. *Dynamics of Adsorption at Liquid Interfaces.* Elsevier. The Netherlands. (1995).

[84] Kennard, E.H. *Kinetic Theory of Gases.* McGraw-Hill. New York. (1938).

[85] Chapman, S and Cowling, T.G. *The Mathematical Theory of Non-Uniform Gases.* Cambridge University Press. London (1970).

[86] Eckbreth, A.C. Effect of Laser-Modulated Particle Incandescence on Raman Scattering Diagnostics. *J Appl Phys.* 48:11:4473-4479. (1977).

[87] McCoy, B.J. and Cha, C.Y. Transport Phenomena in the Rarefied Gas Transition Regime. *Chem Engin Sci.*29:381-388. (1974).

[88] German, R.M. and MWlir, Z.A. Surface Area Reduction During Isothermal Sintering, *J Am Cera Soc.*59:9-10. (1976).

[89] Frenkel, J. *J Phys.* 9:385. (1945).

[90] Hiram, Y and Nir, A. A Simulation of Surface Tension Driven Coalescence. *J Colloid Interf Sci.* 95:2:462-470. (1983).

[91] Koch, W and Friedlander, S.K. The Effect of Particle Coalescence on the Surface Area of a Coagulating Aerosol, *J Colloid Interf Sci.* 140:2:419-427. (1990).

[92] Van Vlack, L.H. *Elements of Material Science and Engineering.* 5th Ed. Adison-Wesley. New York. (1985).

[93] Xiong, Y., Akhtar K., and Pratsinis, S.E. Formation of Agglomerate Particles by Coagulation and Sintering- Part 11. The Evolution of the Morphology of Aerosol-Made Titania, Silica, and Silica Doped Titania Powders. *J Aerosol Sci.*24:3:310-313. (1993).

[94] Friedlander, S.K., and Wu, M.K. Linear Rate Law for the Decay of the Excess Surface Area of a Coalescing Solid Particle. *Phys Rev B.* 49:3622-3624. (1994).

[95] Xiong, Y., Pratsinis, S.E., and Weimer, A.W. Modeling the Formation of Boron Carbide Particles in an Aerosol Flow Reactor. *AIChE J.* 38:11:1685-1692. (1992)

[96] Lyklema, J. *Fundamentals of Interface and Colloid Science.* Vol.l. Academic Press. New York. (1991).

[97] Hunter, R.J. *Foundations of Colloid Science.* Vol. 1. Clarendon Press. New York. (1987).

[98] Hinds, W.C. Physical and Chemical Changes in Particulate Phase. In *Aerosol Measurements, Principles, Techniques and Applications*. Ed. Willeke, K., and Baron, P.A. John Wiley and Sons. New York (1994).